



Showcasing research from Professor Kasper Moth-Poulsen's laboratory, School of Chemical Engineering, Polytechnic University of Catalonia, Barcelona, Spain.

Enhancing the statistical probability factor in triplet-triplet annihilation photon upconversion *via* TIPS functionalization

This work shows the influence of triisopropylsilyl functionalization on annihilators in triplet-triplet annihilation photon upconversion, specifically focusing on their spin statistical probability factor (f). The f determines the probability of singlet generation after triplet coupling. A new green-emitting annihilator 3,9-bis((triisopropylsilyl)ethynyl)perylene (**TIPS-PY**) was synthesized, which shows a high red-to-green TTA-UC quantum yield, $\Phi_{UC} = 13.7\%$ due to high $f = 39.25\%$. Computation analysis revealed that high f of **TIPS-PY**, resulted from enhanced coupling of the triplet-pair state with the singlet state due to high singlet character of the triplet state.

Image reproduced by permission of Lukas Naimovičius and Kasper Moth-Poulsen from *Chem. Sci.*, 2025, **16**, 20255.

As featured in:



See Pankaj Bharmoria,
Kasper Moth-Poulsen *et al.*,
Chem. Sci., 2025, **16**, 20255.

Cite this: *Chem. Sci.*, 2025, **16**, 20255

All publication charges for this article have been paid for by the Royal Society of Chemistry

Enhancing the statistical probability factor in triplet–triplet annihilation photon upconversion via TIPS functionalization

Lukas Naimovičius,^{id}^{abc} Manvydas Dapkevičius,^b Edvinas Radiunas,^{id}^b Mila Miroshnichenko,^a Gediminas Kreiza,^b Carles Alcaide,^{id}^d Paulius Baronas,^{id}^e Yoichi Sasaki,^f Nobuhiro Yanai,^{id}^f Nobuo Kimizuka,^f Andrew B. Pun,^{id}^c Miquel Solà,^{id}^d Pankaj Bharmoria,^{*a} Karolis Kazlauskas^{id}^b and Kasper Moth-Poulsen^{id}^{*aegh}

We investigated the influence of triisopropylsilyl (TIPS) functionalization on annihilators in triplet–triplet annihilation photon upconversion, specifically focusing on their spin statistical probability factor. A new green-emitting annihilator 3,9-bis(triisopropylsilyl)ethynylperylene (TIPS-PY) displaying a record red-to-green TTA-UC quantum yield of 13.7% (50% theoretical maximum) was synthesized. This remarkable efficiency was achieved due to the following features of the TIPS functionalization of PY: (1) retaining a high fluorescence quantum yield of 95%, (2) reduced triplet energy to 1.29 eV enabling efficient triplet energy transfer (~100%) from the sensitizer PdTPBP ($T_1 = 1.55$ eV), and (3) a high efficiency of singlet generation after triplet coupling, indicated by the statistical probability factor, $f = 39.2\% \pm 2.4\%$. Notably, the f value of TIPS-PY surpasses other annihilators in the 470–570 nm emission range. Excited state computational analysis using TheoDORE revealed a higher percentage of charge transfer character in S_0S_1 in TIPS-PY compared to PY, indicative of higher singlet-like character in their triplet-pair state $^1(T_1T_1)$, which can enhance the coupling of the triplet-pair state with the excited singlet-state, thereby increasing the efficiency of singlet generation, a phenomenon undisclosed before. Furthermore, the suitable T_1 of TIPS-PY enables upconversion of 730 nm light when sensitized with $Os(m-pepty)_2(TFSI)_2$ ($T_1 = 1.63$ eV), demonstrating the broad upconversion range of TIPS-PY in the phototherapeutic window desired for biological applications.

Received 15th July 2025
Accepted 6th October 2025

DOI: 10.1039/d5sc05248c
rsc.li/chemical-science

Introduction

Triplet–triplet annihilation photon upconversion (TTA-UC) is a molecular nonlinear optical process that converts two photons with low-energy into one photon with high energy (Scheme 1a).¹

^aInstitute of Materials Science of Barcelona (ICMAB-CSIC), Universitat Autònoma de Barcelona, Bellaterra, Barcelona, 08193, Spain. E-mail: kasper.moth-poulsen@upc.edu; pbharmoria@icmab.es

^bInstitute of Photonics and Nanotechnology, Vilnius University, Saulėtekio av. 3, LT-10257 Vilnius, Lithuania

^cDepartment of Chemistry and Biochemistry, University of California San Diego, 92093 La Jolla, CA, USA

^dInstitute of Computational Chemistry and Catalysis (IQCC) and Department of Chemistry, Universitat de Girona, M. Aurèlia Capmany 69, 17003 Girona, Spain

^eDepartment of Chemical Engineering, Universitat Politècnica de Catalunya EEBE Eduard Maristany 10–14, 08019 Barcelona, Spain

^fDepartment of Applied Chemistry, Graduate School of Engineering Kyushu University 744 Moto-oka, Nishi-ku, Fukuoka 819-0395, Japan

^gCatalan Institution for Research & Advanced Studies (ICREA), Pg. Lluís Companys 23, Barcelona, Spain

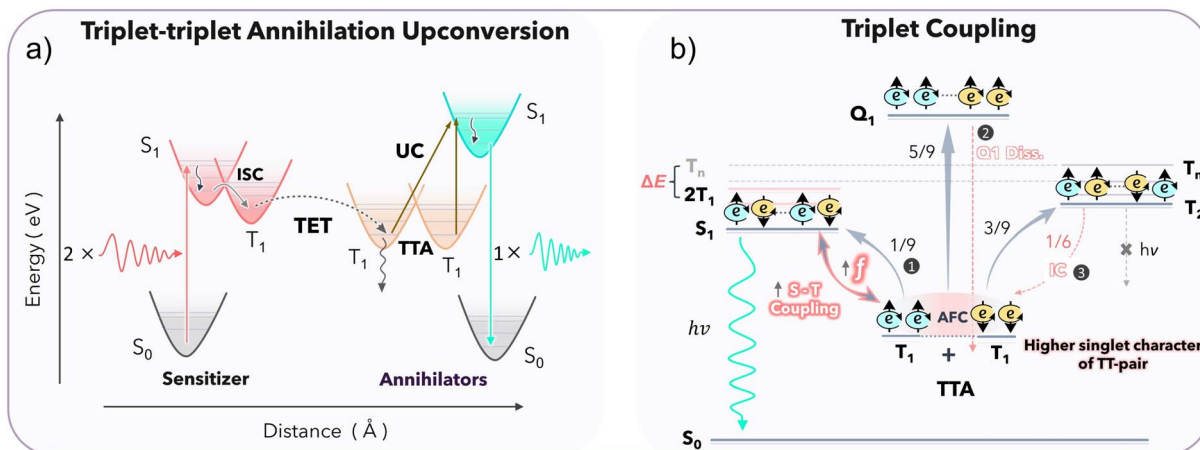
^hDepartment of Chemistry and Chemical Engineering, Chalmers University of Technology, Kemivägen 4, Gothenburg 412 96, Sweden

This phenomenon is attractive compared to other UC processes² due to its operation under incoherent low energy density excitations³ which opens many potential applications such as photocatalysis, biological photoactivation, 3D printing, and photovoltaics.^{4–11} A typical TTA-UC system consists of a sensitizer and an annihilator ensemble. The sensitizer absorbs low-energy photons and generates triplet states *via* intersystem crossing (ISC). The annihilator accumulates the triplets through Dexter triplet energy transfer (TET) from the sensitizer and undergoes TTA-UC, generating a photon-emitting high-energy singlet state (Scheme 1a). The efficiency of singlet generation is evaluated by TTA-UC quantum yield (ϕ_{UC}), which is the product of all operational processes within the TTA-UC system (eqn (1)) and the spin-statistical probability factor (f). The f determines the probability of singlet generation after triplet coupling (Scheme 1b).

$$\phi_{UC} = \frac{1}{2}f\phi_{ISC}\phi_{TET}\phi_{TTA}\phi_{FL} \quad (1)$$

In the eqn (1), ϕ_{UC} , ϕ_{ISC} , ϕ_{TET} , ϕ_{TTA} , ϕ_{FL} represent the quantum yields of upconversion (UC), intersystem crossing (ISC), triplet





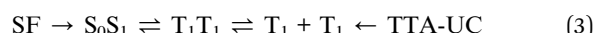
Scheme 1 (a) Scheme of TTA-UC indicating conversion of two low-energy photons into one high-energy photon through a series of energy transfer processes. ISC – intersystem crossing, TET – triplet energy transfer, TTA – triplet–triplet annihilation and UC – upconversion (b) schematic illustration of the post-TTA events resulting in the formation of the TT pair with singlet (S_1 , $f = 1/9$), triplet (T_2 , $3/9$) and quintet (Q_1 , $5/9$) states due to the anti-ferromagnetic coupling (AFC) between triplet-pairs. Further recycling via quintet dissociation (Q1 diss.) or internal conversion (IC) can increase the f of S_1 formation to $1/2$. A higher singlet character of the TT pair increases the coupling between the TT pair and the singlet state, which further increases the f .

energy transfer (TET), triplet–triplet annihilation (TTA), and annihilator fluorescence (FL), respectively.

The f plays an essential role in TTA-UC by defining the maximum achievable ϕ_{UC}^∞ as $f/2$ when all other processes approach unity. As follows, the f allows us to assess the intrinsic potential of the annihilator triplets to generate an emissive singlet state (Scheme 1b). It can be altered by suitable molecular engineering of annihilator chromophores to control the triplet coupling strength, which has been investigated in this work. The TTA results in the formation of a triplet-pair ($T_1 \cdots T_1$) whose net spin can be $S = 0, 1$, or 2 , hence possessing singlet, triplet, or quintet character. According to the adapted Merrifield model including exchange interactions (J), under zero-field splitting, coupling results in the formation of 9 spin eigenstates of $T_1 T_1$ pairs with an overall fraction of $1/9$, $3/9$, and $5/9$ of singlet, triplet, and quintet pair states (Scheme 1b). Triplet coupling can be expressed simply by Heisenberg's spin-only Hamiltonian (\hat{H}) using eqn 2

$$\hat{H} = -2J\hat{S}_1 \cdot \hat{S}_2 \quad (2)$$

where \hat{S}_1 and \hat{S}_2 are individual spin operators of the two individual interacting triplets, and J is the magnetic exchange parameter that also defines the strength of inter-triplet exchange interactions.^{1,5} In the case of strong electronic coupling, the quintet state (Q_1) is energetically inaccessible and cannot form the excited singlet state. This limits the f of singlet formation to $1/4$, leading to low UC efficiencies. However, the quintet and triplet (T_2) states may re-participate in singlet formation via other channels like Q_1 to T_1 dissociation, and T_2 to T_1 internal conversion (IC).^{12,13} This recycling can increase the experimentally obtained f value even up to $\sim 1/2$.^{5,14,15} The TTA-UC (${}^1(T_1 T_1) > S_1 S_0$) is the reverse process of singlet fission ($S_1 S_0 > {}^1(T_1 T_1)$) with an intermediate correlated triplet-pair state, ${}^1(T_1 T_1)$ as per the Johnson–Merrifield model eqn (3).^{16,17}



It is according to the Merrifield model that the singlet character of the $T_1 T_1$ pair determines its coupling to the singlet state.¹⁸ Hence, annihilators with a triplet-pair state exhibiting a significant singlet character can have a high probability of singlet formation and consequently, a higher f factor¹⁹ which has been investigated in this work by calculating the percentage of charge resonance/transfer character in the $S_0 S_1$ dimer.

Another way to increase the f factor is to avoid secondary loss channels such as $2T_1$ to T_n non-radiative decay (Scheme 1b). This can be achieved via the molecular engineering of an annihilator with $2T_1 \approx S_1$ and Q_n and T_n states higher in energy than the $2T_1$ state. This prevents $2T_1$ decay to Q_n or T_n states due to the energy gap law relation⁵ (eqn (3)). This results in preferential decay of $2T_1$ to the S_1 state, leading to more efficient singlet generation.

$$k_{nr} \sim \exp\left(\frac{-\gamma|\Delta E|}{\hbar\omega_M}\right) \quad (4)$$

where k_{nr} is the rate of non-radiative decay and ΔE is the energy gap between electronic states.

Several derivatives of naphthalene,^{14,20} anthracene,^{21–23} perylene,^{24,25} rubrene,^{26–30} and diketopyrrolopyrrole^{31,32} based compounds have been investigated to achieve high f values to boost the overall ϕ_{UC}^∞ .⁵ The UC emission of these compounds spans across the majority of the UV-visible spectrum. However, the lack of an efficient annihilator emitting within the 470–540 nm range impedes important biological applications which can be photoactivated with upconverted green light upon excitation within or close to the phototherapeutic window (650–850 nm).³³ These applications include targeted drug delivery,³⁴ light-gated ion channel control,³⁵ light-activated CRISPR,³⁶ photo-pharmacology,³⁷ and photosynthesis.³⁸ While 9,10-



bis(phenylethynyl)anthracene (**BPEA**) is a well-known commercially available green annihilator, its low UC quantum yield due to the small $f = 5.6$ to 6.3% is an issue.²¹ Therefore, an efficient annihilator within the 470–540 emission range could serve as a powerful photoactivation tool in biological applications upon low-density red or NIR excitation *via* TTA-UC for embracing higher penetration into biological tissue.

Herein, we report the synthesis of a new perylene (**PY**) based annihilator functionalized with triisopropylsilyl (TIPS) groups, **TIPS-PY** (Fig. 1a). **TIPS-PY** demonstrates highly efficient TTA-UC, with experimental ϕ_{UC} of 13.7% (out of 50%), with $f = 39.2\%$ upon combining with $Pd(n)$ *meso*-tetraphenyl tetra-benzoporphine (**PdTPBP**) as sensitizer ($\lambda_{ex} = 640$ nm CW laser). The ϕ_{UC} is shown to be greater compared to unfunctionalized **PY** due to the increase in f value implying enhanced triplet-pair-singlet coupling, which may be governed by the singlet-like character of the triplet-pair state of **TIPS-PY**, revealed from the higher percentage charge resonance or charge transfer character of the S_0S_1 excitations of the **TIPS-PY** compared to **PY**

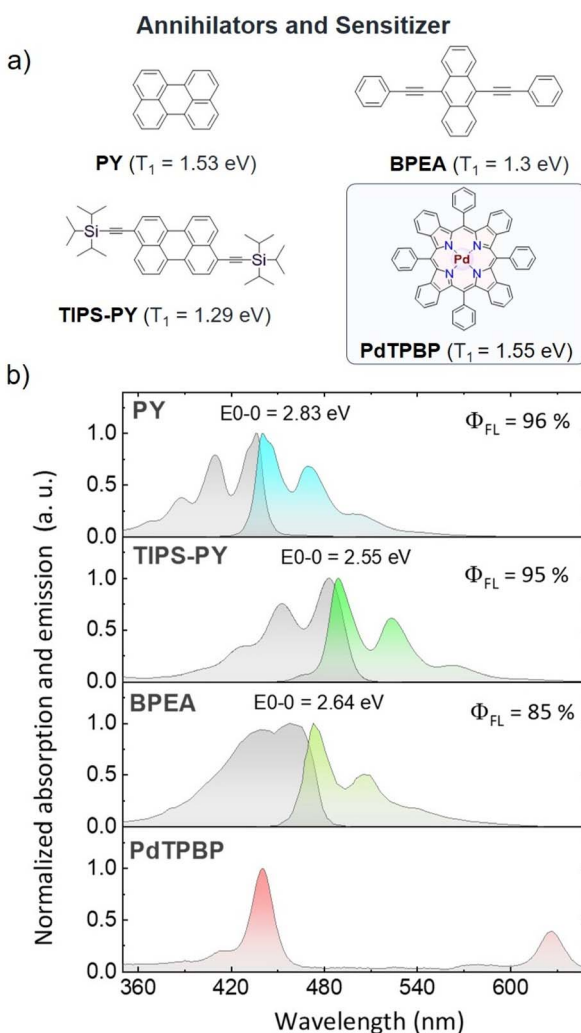


Fig. 1 Molecular structures and T_1 energies (a), and absorption and emission spectra (b) of annihilators (PY, TIPS-PY, BPEA), and sensitizer (PdTPBP) at concentrations of $20\ \mu M$ and $1\ \mu M$ in THF, respectively.

using TheoDORE program.^{19,39} To our knowledge, an efficient annihilator in 470–540 nm emission range with a high f value of $39.2\% \pm 2.4\%$ and ϕ_{UC}^∞ up to 19.6% (theoretical limit) has not been reported before.⁴⁰ This study demonstrates the value of TIPS-functionalization in engineering the triplet energy, singlet-triplet character, and T_1T_1 coupling of annihilator triplets to yield a high statistical probability factor for upconverted singlet-state generation, which is a key limiting factor in TTA-UC. When combined with $Os(m-peptyp)_2(TFSI)_2$ as a sensitizer, **TIPS-PY** upconverted the 730 nm light into yellow-green light, thus reaching deep into the phototherapeutic window³³ that is highly sought after for various biological applications.^{34–38}

Results and discussion

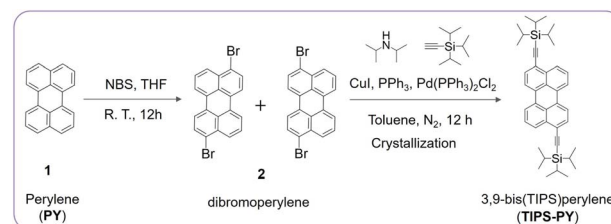
Synthesis of 3,9-bis((triisopropylsilyl)ethynyl)perylene (TIPS-PY)

The annihilator **TIPS-PY** was synthesized in a two-step reaction as depicted in Scheme 2. A mixture of 3,9- and 3,10-dibromoperylene was obtained *via* an electrophilic aromatic bromination reaction between **PY**, and *n*-bromosuccinimide (**NBS**).⁴¹ The final compound, **TIPS-PY**, was obtained *via* a Sonogashira coupling between the mixture of 3,9- and 3,10-dibromoperylene and TIPS-acetylene. The purified-orange colored compound was characterized by 1H NMR, ^{13}C { 1H } NMR, MALDI-TOF, and single-crystal X-ray diffraction analysis (for detailed synthesis procedure and characterization see Annexure 1, Fig. S1–S5) and found to be 3,9-bis(TIPS)perylene.

Photophysical properties

The photophysical properties of **TIPS-PY** were studied in comparison to other competitive annihilators, **PY** and **BPEA** in the 470 to 540 nm emission range. The molecular structures of **TIPS-PY**, **PY**,⁴² and **BPEA** (ref. 21) are shown in Fig. 1a along with **PdTPBP**, the sensitizer used in this study for red-to-green upconversion.⁴³

TIPS-PY demonstrated absorption and emission peaks at 483 nm ($\epsilon \sim 73\,000\text{ M}^{-1}\text{ cm}^{-1}$, Fig. S6) and 489 nm ($\phi_{FL} = 95\%$ and $\tau_{FL} = 5.5\text{ ns}$), respectively (Fig. 1b, S7, and S8). Compared to **PY**, the emission spectrum of **TIPS-PY** is red-shifted by 0.29 eV due to the extension of conjugation upon introduction of TIPS-acetylene moieties (Fig. 1b). However, the ϕ_{FL} remained almost the same (96% and 95%). This red shift in the emission spectrum of **TIPS-PY** overcame the secondary inner filter issue caused by reabsorption of UC light by the **PdTPBP** Soret band to



Scheme 2 Synthesis of 3,9-bis(TIPS)perylene (TIPS-PY).



boost the ϕ_{UC} (Fig. S9). When compared to **BPEA**, the emission spectrum of **TIPS-PY** is red-shifted by just 0.1 eV (Fig. 1b). However, the lower $\phi_{FL} = 85\%$ ²¹ of **BPEA** implies a negative effect on the overall ϕ_{UC} according to eqn (1). Besides ϕ_{FL} , our previous time-dependent density functional theory (TD-DFT) investigations (Gray *et al.*²¹) found that the difference in geometry of singlet and triplet surfaces of **BPEA** makes the triplet-state energetically inefficient to generate the first excited singlet-state to yield low ϕ_{UC} .²¹ Hence, prior to TTA-UC experiments, molecular geometry optimization, and excited state modeling studies of **TIPS-PY** in comparison to **PY** were conducted (Fig. 1 and S10).

Excited-state modeling studies

The DFT and TD-DFT calculations carried out at the (U)PBE0-D3(BJ)/6-311G(d,p) level of theory have shown the T_1 states of **PY** and **TIPS-PY** at 1.49 eV and 1.29 eV, respectively (see SI for a more detailed description of the computational method). The calculated T_1 of **PY** is almost similar to the reported experimental⁸ and theoretical values \sim 1.5 eV.⁴² The calculated singlet-state (S_1) energies of **PY** and **TIPS-PY** (Fig. S10) are also in agreement with the experimental S_1 values. Due to the T_1 of **TIPS-PY** at 1.29 eV, **PdTPBP** having T_1 at 1.55 eV⁴² (Fig. 1a) was selected as a sensitizer to ensure the feasible sensitization of **TIPS-PY** via an exothermic triplet energy transfer pathway. Moreover, the non-overlapping of the emission spectrum of **TIPS-PY** with the absorption spectrum of **PdTPBP** (Fig. 1b and S9), and a high ϕ_{ISC} of **PdTPBP** approaching unity⁴⁴ were other key factors for **PdTPBP** selection as a sensitizer.

The calculated energy level distributions (Fig. S10) demonstrate that **TIPS-PY** complies with the $2T_1 > S_1$ energetic condition for TTA-UC to occur.⁵ However, the proximity of $2T_1$ to higher energy triplet-states ($T_n = T_2, T_3$) plays a crucial role in the probability of singlet generation due to the energy gap law relation (eqn (4)), imposing a non-radiative decay channel if $2T_1$ is in the vicinity of T_2 and further from S_1 .^{45,46} We investigated the implication of the energy gap law in affecting the f factor of **TIPS-PY** and found a $2E_{T_1} - E_{T_2}$ energy gap of +70 meV. The gap is significant enough to substantially reduce the non-radiative decay.⁴⁵⁻⁴⁷ Hence, it could be one of the key contributors to the high f factor of **TIPS-PY**. However, when compared with the $2E_{T_1} - E_{T_2} = -140$ meV of **PY** having f value of 17.9%,⁴² this parameter does not seem enough to explain the high f factor observed of **TIPS-PY**. Hence, we explored another possible channel to understand the high f factor of **TIPS-PY**. One key argument of the Merrifield model of triplet-triplet coupling is that the efficiency of singlet generation depends on the triplet pair-singlet coupling.^{18,29,48} Hence, a higher singlet character of the triplet-state can increase the singlet-triplet coupling post triplet-triplet annihilation to generate a high singlet population.¹⁸ Therefore, we calculated the charge resonance or charge transfer character of S_1S_0 , commonly shared by $^4(T_1T_1)$, of **TIPS-PY** compared to that of **PY** to assess the singlet character using TheoDORE program (Fig. 2).³⁹ Fig. 2a shows the change in electron density from the ground state to the excited state, resulting from a linear combination of orbital replacement

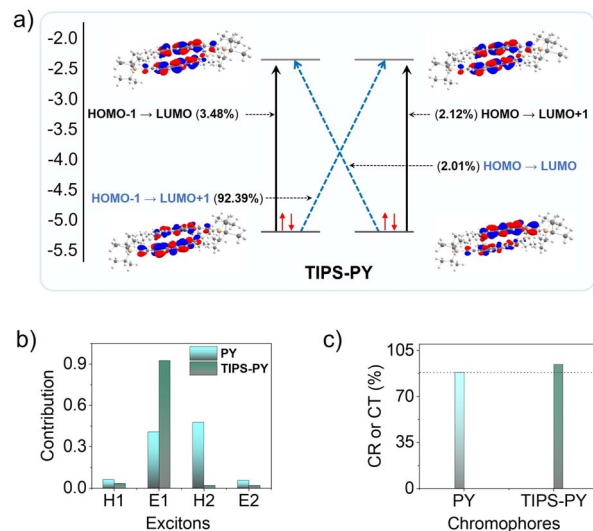


Fig. 2 (a) Illustration of the contribution of the linear combination of orbital replacement in **TIPS-PY**. (b) Plot showing comparative electron (E), and hole (H) contributions during orbital replacement in **PY** and **TIPS-PY**. (c) Percentage of charge resonance (CR) or charge transfer (CT) calculated from E and H contributions during orbital replacement in **PY** and **TIPS-PY**.

involving charge transfer (blue arrows) and local excitations (black arrows). The HOMO-1 to LUMO+1 transition in **TIPS-PY**, which contributes the strongest (92.39%), has charge transfer (CT) character, moving one electron each from left to right and from right to left. Contrary to this, the HOMO-1 to LUMO+1 transition in **PY**, which contributes the strongest (88.24%), has a charge resonance (CR) character. The percentage of CT or CR character is indicative of the singlet character of the dimer.³⁹ These results indicate that TIPS-functionalization increases the singlet character of the **TIPS-PY** dimer, which is likely to have a positive effect on f value (Scheme 1b)^{16,49-51} and UC quantum yield.

To substantiate these results, we also investigated biphenyl (**BP**) and bis-TIPS-biphenyl (**TIPS-BP**), having a similar transition dipole axis as that of **PY** (Fig. S11a and b)^{52,53} using the TheoDORE program (Fig. S12). Similar to **PY**, the CT character of **BP** increased upon TIPS-functionalization (Fig. S12d), thus supporting the proposed argument. Recently, **TIPS-BP** was shown to demonstrate superior UC performance compared to **BP**, confirming our prediction experimentally.⁵⁴ Seeking further generalization of this argument, we also calculated the CT or CR character for highly efficient TIPS-functionalized annihilators such as TIPS-anthracene (**TIPS-An**) (ref. 23) and TIPS-naphthalene (**TIPS-Naph**).⁵⁵ However, the CT or CR character decreased for these molecules upon TIPS-functionalization (Fig. S13a-d). This could be due to the difference in the main transition dipole axis of **Naph** and **An** ($^1L_\alpha$), which unlike **BP** and **PY** is along the horizontal axis (Fig. S11b). It is to mention that the transition dipole axis plays a key role in the electronic interactions of the molecules in the excited state.⁵⁶ Nevertheless, it shows that the singlet character of the triplet pair may not be the sole criterion to evaluate the high TTA-UC quantum

yields in molecules with different transition dipole axes. Therefore, we also investigated the role of energy gap law⁵ in **TIPS-An** and **TIPS-Naph** and found $2E_{T_1} - E_{T_2}$ of -103 meV, and $+186$ meV, respectively (Table S2), which is in synergy with results obtained upon application of the energy gap law in the case of **PY** and **TIPS-PY**. Therefore, the energy gap law could be the common factor contributing to high ϕ_{UC} (27%)²³ of **TIPS-An** and high f value (54%)⁵⁵ of **TIPS-Naph** chromophores, as well as **TIPS-PY**. Seeking further insights, we also computed the S_0S_0 and T_1T_1 states for **PY** and **TIPS-PY** and found a smaller dimerization energy for **TIPS-PY** (-31.6 kcal mol⁻¹) compared to that of **PY** (-20.43 kcal mol⁻¹) (see Fig. S14).⁵⁷ In both cases, the potential energy surface is relatively flat, allowing for easy rotation and translation of the dimers. In the particular case of **PY**, we have also computed the S_0S_1 , S_0T_1 , S_0T_2 , and T_1T_2 states (Fig. S15). As the emission of **TIPS-PY** is red-shifted due to the presence of TIPS moieties, the extended conjugation leads to a decrease of excited state energies (Fig. 1a) as well as the polarization of the $C\equiv C$ bond in the opposite direction by the triplet spin compared to **PY** (Fig. S16). The higher stability of the T_1 state in **TIPS-PY** can be attributed to the reduction of the HOMO–LUMO gap by 0.37 eV in **TIPS-PY** compared to **PY**.⁵⁷ Given the extension of conjugation, the T_1 energy of **TIPS-PY** (1.29 eV) decreased by 0.24 eV compared to **PY** (1.53 eV) making it suitable for exothermic triplet-energy transfer.

Triplet–triplet annihilation photon upconversion

Following photophysical characterization and excited-state modeling studies, the **TIPS-PY** annihilator was applied in TTA-UC in combination with **PdTPBP** as a sensitizer in deaerated THF. The investigated **TIPS-PY**: **PdTPBP** UC system demonstrated UC emission upon 640 nm laser excitation (Fig. 3a, b and S17), confirming the DFT prediction of the most favourable energetic condition ($2T_1 \geq S_1$) for TTA-UC.⁵ To demonstrate the full potential of **TIPS-PY**, the annihilator concentration was varied from 0.1 mM to 100 mM while the **PdTPBP** concentration was maintained at 0.01 mM (Fig. 3a and c). The **TIPS-PY**: **PdTPBP** system demonstrated a high experimental ϕ_{UC} varying from 7.0% to 13.7% (Fig. 3c and Table 1) at 100 mM and 1 mM annihilator concentrations, respectively. The ϕ_{UC}^∞ and UC threshold (I_{th}) were estimated from ϕ_{UC} vs. excitation power density (I_{ex}) profile according to previously reported procedures⁵⁸ (Fig. S18 and Table 1).

The I_{th} values for **TIPS-PY**: **PdTPBP** vary from 0.19 W cm⁻² to 0.43 W cm⁻², a low threshold barrier desired for most applications. The difference in ϕ_{UC}^∞ at varying **TIPS-PY** concentrations can be explained by concentration effects on ϕ_{FL} and ϕ_{TET} according to eqn (1). While the ϕ_{FL} (75.5% – 73.5%) for 0.1 mM to 10 mM concentrations are similar, the 100 mM concentration sample demonstrates a decrease in ϕ_{FL} to 65.5% owing to the aggregation of the annihilator species (Fig. 3a and S19). This suggests an enhanced non-radiative decay channel, potentially due to the aggregation. It was also reflected in the anti-Stokes shifts, which varied from 0.56 to 0.21 eV between 0.1 to 100 mM **TIPS-PY** (Table S3).⁵⁹ No significant aggregation is observed up to a concentration of 10 mM, as evidenced by the

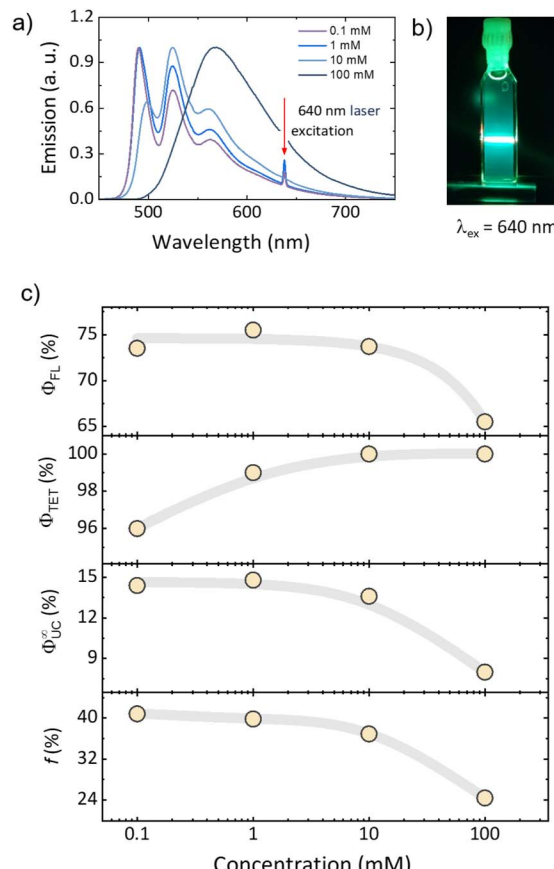


Fig. 3 (a) **TIPS-PY**: **PdTPBP** upconversion spectra at 0.1 mM, 1 mM, 10 mM, and 100 mM annihilator concentrations. 640 nm laser excitation indicated. (b) Digital image of TTA-UC emission, and (c) ϕ_{FL} , ϕ_{TET} , ϕ_{UC}^∞ , and f dependence on **TIPS-PY** concentration. All solutions were prepared in deaerated THF. **PdTPBP** concentration in all UC solutions was maintained at 0.01 mM. The grey lines serve as a guide to the eyes.

absence of changes in the low-energy shoulder of the absorption spectra (Fig. S20). The growth of ϕ_{TET} from 96% to 100% is explained by the higher concentration of acceptor chromophores surrounding sensitizer molecules. The longest triplet-lifetime, $\tau_T = 1250$ μ s was observed at the lowest **TIPS-PY** concentration (0.1 mM), and decreased further upon increasing the concentration (Table 1 and Fig. S21).

This decreases the average distance between **PdTPBP** and **TIPS-PY**, inferring higher TET probability. ϕ_{TET} was evaluated via rise time (τ_r) of TTA-UC transients (Fig. S22 and Table S4) according to the following relation:

$$\phi_{TET} = 1 - \frac{2\tau_r}{\tau_0} \quad (5)$$

where τ_0 – intrinsic (unquenched) triplet lifetime of the sensitizer that, in the case of **PdTPBP**, is 175.5 μ s.⁴² A high $\phi_{TET} = 96\%$ was also confirmed from the quenching of the phosphorescence spectrum of **PdTPBP** by **TIPS-PY** (Fig. S22).

To further understand the higher TTA-UC quantum yields obtained with **TIPS-PY**, the f value of $39.2\% \pm 2.4\%$ was evaluated according to eqn (1) as the average of 3 measurements at

Table 1 UC parameters of TIPS-PY-PdTPBP UC solutions in deaerated THF at 0.1 mM, 1 mM, 10 mM, 100 mM, and 0.01 mM concentrations of TIPS-PY and PdTPBP

TIPS-PY	ϕ_{FL}^a , %	ϕ_{UC}^b , %	$\phi_{\text{UC}}^{\infty c}$, %	ϕ_{TET}^d , %	I_{th}^e , W cm $^{-2}$	τ_T^f , μs	f^g , %
0.1 mM	73.5	11.1	14.4	96	0.19	1250	40.8
1 mM	75.5	13.7	14.9	99	0.29	914	39.8
10 mM	73.7	13.0	13.6	100	0.43	741	36.9
100 mM	65.5	7.0	8.0	100	4.94	30–80	24.4

^a FL quantum yield of annihilator in UC solution. ^b Reabsorption corrected maximum measured UC quantum yield values. ^c Maximum attainable UC quantum yield values. ^d TET quantum yield. ^e UC threshold at 38.2% of $\phi_{\text{UC}}^{\infty}$. ^f Triplet lifetime ($=2 \times \tau_{\text{UC}}$). ^g Statistical probability of singlet generation from two triplets *via* TTA, calculated according to eqn (1). τ_{UC} values in Table 1 were determined from the tail fit of the UC emission decay profiles in Fig. S21.

0.1 mM, 1 mM, and 10 mM annihilator concentrations (Fig. 3b and Table 1). The results obtained at 0.1 mM, 1 mM, and 10 mM support that f value is an intrinsic property of a molecule that does not experience a change due to the change in concentration. The f value of 24.4% recorded at 100 mM was omitted from the calculation due to the presence of **TIPS-PY** aggregates (Fig. 3a and S19) in the UC solution enabling non-radiative decay channels.

For a reliable comparison of f values between studied **PY**,⁴² **TIPS-PY**, and **BPEA**, we conducted additional measurements at identical conditions with **BPEA:PdTPBP** UC system to determine the f value resulting in 6.3% (Fig. S23, S24, and Table S6). The reported f value of $39.2\% \pm 2.4\%$ for **TIPS-PY** outperforms all previously studied annihilators within the 470–570 nm emission region and is among the top values in the entire spectrum (Fig. 4).^{5,40,54,60–62} This leads to a high experimental ϕ_{UC} of 13.7% with a possibility to approach the intrinsic limit $\phi_{\text{UC}}^{\infty} \sim 19.6\%$ if all energy transfer processes approach unity. The main reason for the high f value of **TIPS-PY** is the TIPS functional groups, which increase the stability of the triplet state as well as form a singlet-like character of the triplet dimer (T_1T_1) species, as revealed from the charge resonance or charge

transfer studies. This may exhibit a positive impact on $\text{T}_1\cdots\text{T}_1$ pair state and S_1 coupling to generate the singlet-state with high efficiency according to the Merrifield model.^{18,29,48} Additionally, the favourable energy distribution prevents 2T_1 -to- T_2 non-radiative decay from favouring the S_1 formation.

We also investigated the rate of TTA (k_{TTA}) as a possible reason for higher UC performance in **TIPS-PY** compared to **PY** in THF. To determine k_{TTA} of **TIPS-PY**, UC intensity decay profiles of **TIPS-PY: PdTPBP** and **PY: PdTPBP** solutions containing 0.1 mM of annihilator were measured at increasing excitation power densities (Fig. 5) and fitted using the following relation,⁶³

$$I(t) \left[\propto {}^3A^*(t) \right]^2 = \left([{}^3A^*]_0 \frac{1 - \beta}{\exp(t/\tau_T) - \beta} \right)^2 \quad (6)$$

$$\beta = \frac{2k_{\text{TTA}}[{}^3A^*]_0}{2k_{\text{TTA}}[{}^3A^*]_0 + k_T} \quad (7)$$

Here, $[{}^3A^*]_0$ denotes the initial triplet exciton concentration within the annihilator, and $\tau_T (=1/k_T)$ is the spontaneous triplet decay lifetime. τ_T was obtained from the tails of the transients, assuming that the condition $k_T \gg k_{\text{TTA}}[{}^3A^*]_0$ is met at low triplet exciton concentration, where TTA is negligible.

The obtained β values, which describe TTA efficiency at particular excitation densities, are listed in Table S5, along with

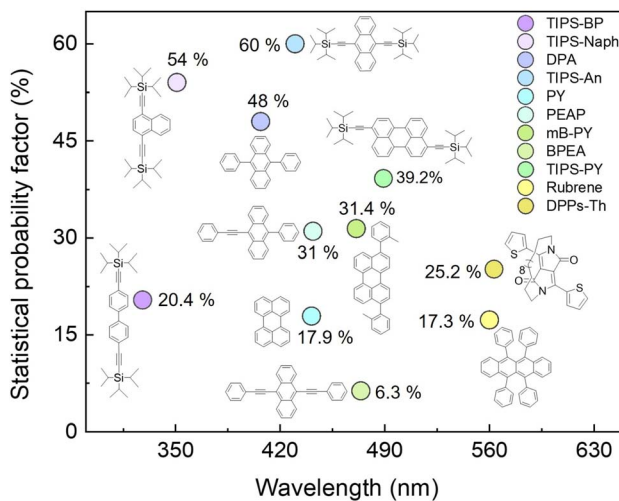


Fig. 4 Plot showing variation in statistical probability factor of various annihilators emitting across the visible spectral range. **TIPS-PY** synthesized in this work tops the list in the 470–570 nm range.

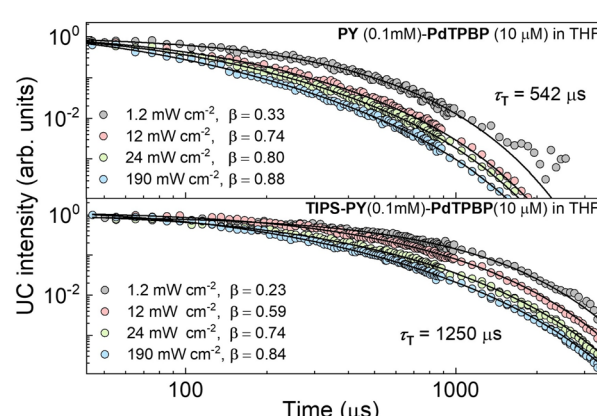


Fig. 5 Normalized UC transients of **PY** and **TIPS-PY** on a log–log scale at different excitation densities (indicated) upon sensitization with **PdTPBP** at 640 nm. Circles present experimental data, while solid lines show global fits with a shared τ_T .



τ_T values. Since pulsed nanosecond excitation with a pulse duration much shorter than triplet lifetime was used, quasi-steady-state conditions could not be achieved, preventing direct determination of $[{}^3A^*]_0$ from these measurements. However, given that the τ_T is known and remains invariant with excitation density, $[{}^3A^*]_0$ at each pump level was estimated utilizing the reported k_{TTA} value for PY ($19 \times 10^8 \text{ M}^{-1} \text{ s}^{-1}$ (ref. 64) according to the eqn (7). Considering the similar TET efficiencies for PY: PdTPBP ($\phi_{TET} = 92\%$)⁴² and TIPS-PY: PdTPBP ($\phi_{TET} = 96\%$; this work) at equivalent annihilator and sensitizer concentrations, the $[{}^3A^*]_0$ values derived for PY: PdTPBP were also employed to estimate k_{TTA} in TIPS-PY. The estimated k_{TTA} for TIPS-PY is approximately $5 \times 10^8 \text{ M}^{-1} \text{ s}^{-1}$, which is 4-fold lower than that of PY. Hence, k_{TTA} may not be the reason for higher UC performance in TIPS-PY compared to PY. This observation is different from what has been reported by Han *et al.*⁴⁰ where the higher normalized triplet-triplet annihilation efficiency of 3,10-di-*o*-tolylperylene (mB-PY) triplets, due to the restricted motion of *o*-tolyl rings was cited as the key reason for enhanced UC quantum yield.⁴⁰ Nevertheless, the enhancement of UC performance by TIPS groups provides a novel strategy for molecular design for future annihilators as well as demonstrates the potential of TIPS-PY as another suitable compound to be implemented in numerous applications, especially in biology requiring 470–540 nm emission upon excitation with deep tissue penetrative red/far-red light.

To further demonstrate the potential of the TIPS-PY for long-wavelength far-red light upconversion, we performed TTA-UC study by combining TIPS-PY with Os(m-peptyl)₂(TFSI)₂ as sensitizer in deaerated DMF (Fig. 6a). The absorption spectrum of Os(m-peptyl)₂(TFSI)₂ shows vibronic peaks at 291, 318, 422, 447 nm due to ligand centred, at 494 nm due to singlet metal-to-ligand charge transfer (¹MLCT), and at 648 nm and 673 nm due to triplet MLCT (³MLCT) (Fig. 6b).⁶⁵ Furthermore, Os(m-peptyl)₂(TFSI)₂ shows ³MLCT emission at 759 nm (1.63 eV) and phosphorescence emission due to meta-substituted perylene units at 827 nm (1.5 eV), respectively.⁶⁵ Unlike other Os-complexes, it shows a long phosphorescence lifetime (τ_{Ph}) of 98 μs (Fig. S25), which is among the key requirements for an efficient sensitizer in TTA-UC.⁵ Upon excitation with a 730 nm CW laser, the TIPS-PY:Os(m-peptyl)₂(TFSI)₂ (1 mM:0.01 mM) system demonstrated bright yellow-green UC emission (Fig. 6c and d), thus expanding the upconversion range into the phototherapeutic window to the far-red region.³³ The phosphorescence transients (Fig. S25) were used to determine the $\phi_{TET} = 99.7\%$, indicating almost complete quenching of TIPS-PY:Os(m-peptyl)₂(TFSI)₂ phosphorescence by TIPS-PY. Despite the high ϕ_{TET} , long triplet lifetime, $\tau_T = 846 \mu\text{s}$ (Fig. S26) and high $\phi_{FL} = 71\%$ of TIPS-PY in this system, a low absolute $\phi_{UC} = 0.62\%$ was observed. This could be due to 1) the secondary inner filter effect caused by fast reabsorption of the upconverted light by Os(m-peptyl)₂(TFSI)₂ due to the high spectral overlap of its absorption spectrum with the emission spectrum of TIPS-PY (Fig. 6b and Fig. S27), or 2) aggregated UC emission due to complexation of TIPS-PY with Os(m-peptyl)₂(TFSI)₂ confirmed from the distorted UC emission spectrum showing shift in emission maxima to 572 nm in the yellow emission range

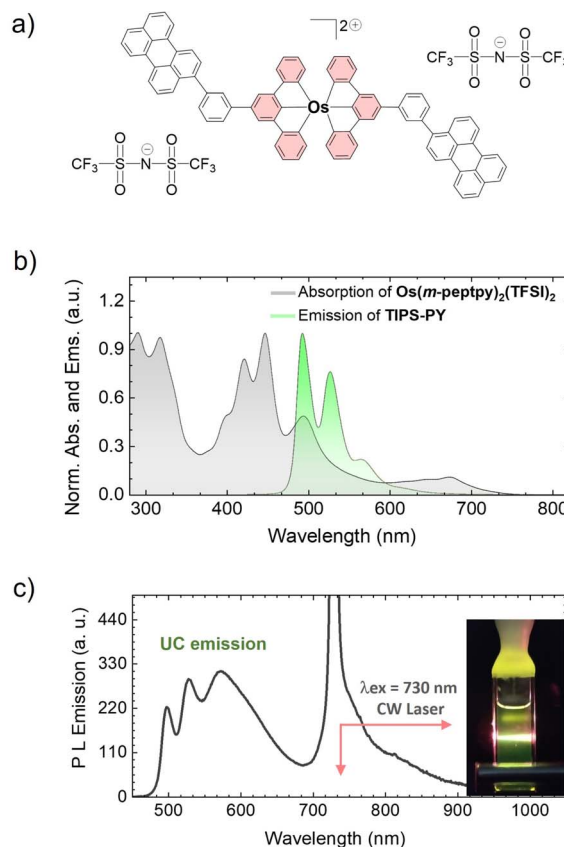


Fig. 6 (a) Molecular structure of Os(m-peptyl)₂(TFSI)₂. (b) Absorption spectrum of Os(m-peptyl)₂(TFSI)₂ (1 mM) in the presence of TIPS-PY (0.01 mM) in DMF ($\lambda_{ex} = 420 \text{ nm}$). (c) Upconversion emission spectrum of TIPS-PY: Os(m-peptyl)₂(TFSI)₂ (1 mM:0.01 mM) system ($\lambda_{ex} = 730 \text{ nm}$ CW laser). (d) Digital image of the yellow-green UC emission upon 730 nm CW laser excitation.

(Fig. 6c). Comparatively low solubility of TIPS-PY in DMF also support the possible aggregated UC emission. A better far-red absorbing sensitizer with higher transparency window in the TIPS-PY emission range may yield higher ϕ_{UC} .

Conclusions

We synthesized a new green-emitting annihilator TIPS-PY, which exhibits the highest absolute TTA-UC quantum yield of 13.7% (50% theoretical maximum) for red-to-green (640 nm to 489 nm) TTA-UC upon combining with PdTPBP as a sensitizer. Such a high UC quantum yield is enabled by the combined effects of: (1) a high $\phi_{FL} = 95\%$ of TIPS-PY, (2) $\phi_{TET} \sim 100\%$ due to exothermic triplet energy transfer from PdTPBP to TIPS-PY, (3) minuscule secondary inner filter effects due to minimum spectral overlap of PdTPBP absorption and TIPS-PY emission, and (4) a high f value of $39.2\% \pm 2.4\%$ of TIPS-PY, which generated a high singlet population after triplet-coupling. Further investigations of the f factor from the TheoDORE program revealed a singlet-like character of the triplet-pair state of TIPS-PY induced by the higher charge transfer character of

the S_0S_1 excitations of **TIPS-PY** compared to **PY**. This may increase the coupling of the triplet-pair state with the excited singlet state of **TIPS-PY** to generate a high singlet population after triplet-triplet annihilation according to the Merrifield model. Interestingly, this behaviour was also observed for other TIPS-functionalized annihilators like **TIPS-BP**, having a similar transition dipole axis to that of **PY**, which was not previously explored. The obtained ϕ_{UC} and f values for **TIPS-PY** are among the highest for annihilators in the green-to-red spectral range and outperform well-known annihilators such as **PY**, **BPEA**, **mBPY**, rubrene, or DPPs.

Author contributions

P. B., L. N., and K. M. P. conceptualized the idea of this work. M.M. synthesized the TIPS-Perylene. P. B. and M. M. carried out primary photophysical characterization. L. N., M. D., E. R., G. K., P. B., and K. K. carried out UC and time resolved measurements. C. A. and M. S. carried out computational calculations. Y. S., N. Y., and N. K. synthesized Os-complex. P.B., L. N., and K. M. P. wrote the first draft of the manuscript. All authors contributed to the analysis of results in their respective parts and editing of the manuscript.

Conflicts of interest

There are no conflicts to declare.

Data availability

The original datasets generated and analyzed during the current study are available from the corresponding authors on reasonable request and also available via open access on Zenodo at <https://doi.org/10.5281/zenodo.37555810>.

Supplementary information: synthesis, NMR, MALDI-TOF, and X-Ray diffraction analysis of TIPS-PY together with photophysical and upconversion measurements and DFT calculations. The authors have cited additional references within the SI.^{66–84} Cartesian coordinates of the species studied for computational calculations. See DOI: <https://doi.org/10.1039/d5sc05248c>.

Acknowledgements

L. N. acknowledges the Erasmus + Traineeship Program, P. B. and M. M. acknowledge financial support from the La-Caixa junior research leadership-post doctoral program (ID: 100010434, fellowship code: LCF/BQ/P122/11910023) the State Investigation Agency, through the Severo Ochoa Programme for Centres of Excellence in R&D (CEX2023-001263-S) and project PID2021-123873NB-I00 for financial support. L. N. and A. B. P. acknowledge the start-up funds provided by the University of California San Diego and the use of facilities and instrumentation supported by NSF through the UC San Diego Materials Research Science and Engineering Center (UCSD MRSEC), grant # DMR-2011924. K. M. P. acknowledges funding from the European Research Council (No. 101002131), the Swedish Energy Agency, the Göran Gustafsson Foundation, the Swedish

Research Council, Swedish Research Council Formas, the European Research Council (ERC) under grant agreement CoG, PHOTHERM – 101002131, the Catalan Institute of Advanced Studies (ICREA), and the European Union's Horizon 2020 Framework Programme under grant agreement no. 951801. M. D., G. K., K. K., acknowledge the "Universities" Excellence Initiative" programme by the Ministry of Education, Science and Sports of the Republic of Lithuania under the agreement with the Research Council of Lithuania (project No. S-A-UEI-23-6). M. S. is grateful for financial support from the Agencia Española de Investigación (MCIN/AEI/10.13039/501100011033) for projects RED2024-154178-T and PID2023-147424NB-I00 and from the Generalitat de Catalunya for Project 2021SGR623 and ICREA Academia 2025 prize to M. S. N. Y. acknowledges the support by JSPS KAKENHI (JP23H00304). N. N. K. acknowledges the support by JSPS KAKENHI (JP20H05676).

References

- 1 P. Bharmoria, H. Bildirir and K. Moth-Poulsen, *Chem. Soc. Rev.*, 2020, **49**, 6529–6554.
- 2 F. Auzel, *Chem. Rev.*, 2004, **104**, 139–174.
- 3 M. Wu, D. N. Congreve, M. W. B. Wilson, J. Jean, N. Geva, M. Welborn, T. Van Voorhis, V. Bulovic, M. G. Bawendi and M. A. Baldo, *Nat. Photonics*, 2016, **10**, 31–34.
- 4 T. Schloemer, P. Narayanan, Q. Zhou, E. Belliveau, M. Seitz and D. N. Congreve, *ACS Nano*, 2023, **17**(4), 3259–3288.
- 5 L. Naimovičius, P. Bharmoria and K. Moth-Poulsen, *Mater. Chem. Front.*, 2023, **7**, 2297–2315.
- 6 B. D. Ravetz, A. B. Pun, E. M. Churchill, D. N. Congreve, T. Rovis and L. M. Campos, *Nature*, 2019, **565**, 343–346.
- 7 Q. Liu, M. Xu, T. Yang, B. Tian, X. Zhang and F. Li, *ACS Appl. Mater. Interfaces*, 2018, **10**, 9883–9888.
- 8 Y. Sasaki, M. Oshikawa, P. Bharmoria, H. Kouno, A. Hayashi-Takagi, M. Sato, I. Ajioka, N. Yanai and N. Kimizuka, *Angew. Chem., Int. Ed.*, 2019, **58**, 17827–17833.
- 9 S. N. Sanders, T. H. Schloemer, M. K. Gangishetty, D. Anderson, M. Seitz, A. O. Gallegos, R. C. Stokes and D. N. Congreve, *Nature*, 2022, **604**, 474–478.
- 10 D. K. Limberg, J. H. Kang and R. C. Hayward, *J. Am. Chem. Soc.*, 2022, **144**, 5226–5232.
- 11 A. J. Carrod, V. Gray and K. Börjesson, *Energy Environ. Sci.*, 2022, **15**, 4982–5016.
- 12 R. E. Merrifield, *J. Chem. Phys.*, 1968, **48**, 4318–4319.
- 13 R. E. Merrifield, *Pure Appl. Chem.*, 1971, **27**, 481–498.
- 14 A. Olesund, J. Johnsson, F. Edhborg, S. Ghasemi, K. Moth-Poulsen and B. Albinsson, *J. Am. Chem. Soc.*, 2022, **144**, 3706–3716.
- 15 A. Monguzzi, R. Tubino, S. Hoseinkhani, M. Campione and F. Meinardi, *Phys. Chem. Chem. Phys.*, 2012, **14**, 4322–4332.
- 16 D. Casanova, Theoretical modeling of singlet fission, *Chem. Rev.*, 2018, **118**, 7164–7207.
- 17 A. J. Carrod, V. Gray and K. Börjesson, *Energy Environ. Sci.*, 2022, **15**, 4982–5016.
- 18 D.-G. Ha, R. Wan, C. A. Kim, T.-A. Lin, L. Yang, T. Van Voorhis, M. A. Baldo and M. Dincă, *Nat. Mater.*, 2022, **21**, 1275–1281.

19 M. B. Smith and J. Michl, *Chem. Rev.*, 2010, **110**, 6891–6936.

20 N. Harada, Y. Sasaki, M. Hosoyamada, N. Kimizuka and N. Yanai, *Angew. Chem., Int. Ed.*, 2021, **60**, 142–147.

21 V. Gray, A. Dreos, P. Erhart, B. Albinsson, K. Moth-Poulsen and M. Abrahamsson, *Phys. Chem. Chem. Phys.*, 2017, **19**, 10931–10939.

22 A. Olesund, V. Gray, J. Mårtensson and B. Albinsson, *J. Am. Chem. Soc.*, 2021, **143**, 5745–5754.

23 D. Beljonne and A. Rao, *ACS Mater. Lett.*, 2019, **1**, 660–664.

24 A. J. Carrod, A. Cravcenco, C. Ye and K. Börjesson, *J. Mater. Chem. C*, 2022, **10**, 4923–4928.

25 C. Ye, V. Gray, K. Kushwaha, S. Kumar Singh, P. Erhart and K. Börjesson, *Phys. Chem. Chem. Phys.*, 2020, **22**, 1715–1720.

26 E. Radiunas, S. Raišys, S. Juršėnas, A. Jozeliūnaitė, T. Javorskis, U. Šinkevičiute, E. Orentas and K. Kazlauskas, *J. Mater. Chem. C*, 2020, **8**, 5525–5534.

27 E. Radiunas, L. Naimovičius, S. Raišys, A. Jozeliūnaitė, E. Orentas and K. Kazlauskas, *J. Mater. Chem. C*, 2022, **10**, 6314–6322.

28 E. Radiunas, M. Dapkevičius, L. Naimovičius, P. Baronas, S. Raišys, S. Juršėnas, A. Jozeliūnaitė, T. Javorskis, U. Šinkevičiūtė, E. Orentas and K. Kazlauskas, *J. Mater. Chem. C*, 2021, **9**, 4359–4366.

29 D. G. Bossanyi, Y. Sasaki, S. Wang, D. Chekulaev, N. Kimizuka, N. Yanai and J. Clark, *JACS Au*, 2021, **1**, 2188–2201.

30 W. S. Y. Cheng, B. Fuckel, T. Khouri, R. G. C. R. Clady, M. J. Y. Tayebjee, N. J. Ekins-Daukes and M. J. Crossley, *J. Phys. Chem. Lett.*, 2010, **1**, 1795–1799.

31 A. B. Pun, L. M. Campos and D. N. Congreve, *J. Am. Chem. Soc.*, 2019, **141**, 3777–3781.

32 L. Naimovičius, E. Radiunas, B. Chatinovska, A. Jozeliūnaitė, E. Orentas and K. Kazlauskas, *J. Mater. Chem. C*, 2023, **11**, 698–704.

33 G. Alachouzos, A. M. Schulte, A. Mondal, W. Szymanski and B. L. Feringa, *Angew. Chem., Int. Ed.*, 2022, **61**, e202201308.

34 A. K. Singh, S. Banerjee, A. V Nair, S. Ray, M. Ojha, A. Mondal and N. D. P. Singh, *ACS Appl. Bio. Mater.*, 2022, **5**, 1202–1209.

35 K. R. Konrad, S. Gao, M. D. Zurbriggen and G. Nagel, *Annu. Rev. Plant Biol.*, 2023, **74**, 313–339.

36 K.-N. Chen and B.-G. Ma, *ACS Synth. Biol.*, 2023, **12**, 1708–1715.

37 S. H. C. Askes, M. Kloz, G. Bruylants, J. T. M. Kennis and S. Bonnet, *Phys. Chem. Chem. Phys.*, 2015, **17**, 27380–27390.

38 I. Terashima, T. Fujita, T. Inoue, W. S. Chow and R. Oguchi, *Plant Cell Physiol.*, 2009, **50**, 684–697.

39 F. Plasser, *J. Chem. Phys.*, 2020, **152**, 084108.

40 L. Zeng, L. Huang, W. Lin, L. H. Jiang and G. Han, *Nat. Commun.*, 2023, **14**, 1102.

41 M. Tracy, S. Singh and Sony Corp, WO2017197144A1, 2016.

42 L. Naimovičius, E. Radiunas, M. Dapkevičius, P. Bharmoria, K. Moth-Poulsen and K. Kazlauskas, *J. Mater. Chem. C*, 2023, **11**, 14826–14832.

43 A. J. Carrod, A. Cravcenco, C. Ye and K. Börjesson, *J. Mater. Chem. C*, 2022, **10**, 4923–4928.

44 J. E. Rogers, K. A. Nguyen, D. C. Hufnagle, D. G. McLean, W. Su, K. M. Gossett, A. R. Burke, S. A. Vinogradov, R. Pachter and P. A. Fleitz, *J. Phys. Chem. A*, 2003, **107**, 11331–11339.

45 R. Englman and J. Jortner, *Mol. Phys.*, 1970, **18**, 145.

46 W. Siebrand, *J. Chem. Phys.*, 1967, **47**, 2411–2422.

47 S. J. Jang, *J. Chem. Phys.*, 2021, **155**, 1641061–1641069.

48 R. C. Johnson and R. E. Merrifield, *Phys. Rev. B*, 1970, **1**, 896–902.

49 M. Gudem and M. Kowalewski, *Chem.-Eur. J.*, 2022, **28**, e202200781.

50 K. C. Krishnapriya, P. Roy, B. Puttaraju, U. Salzner, A. J. Musser, M. Jain, J. Dasgupta and S. Patil, *Nat. Commun.*, 2019, **10**, 33.

51 K. Miyata, F. S. Conrad-Burton, F. L. Geyer and X.-Y. Zhu, *Chem. Rev.*, 2019, **119**, 4261–4292.

52 H.-S. Im and E. R. Bernstein, *J. Chem. Phys.*, 1988, **88**, 7337–7347.

53 P. Yan, A. Chowdhury, M. W. Holman and D. M. Adams, *J. Phys. Chem. B*, 2005, **109**, 724–730.

54 J. A. Moghtader, M. Uji, T. J. B. Zähringer, M. Schmitz, L. M. Carrella, A. Heckel, E. Rentschler, N. Yanai and C. Kerzig, *ChemRxiv*, 2025, DOI: [10.26434/chemrxiv-2025-9ppr7](https://doi.org/10.26434/chemrxiv-2025-9ppr7).

55 A. Olesund, J. Johnsson, F. Edhborg, S. Ghasemi, K. Moth-Poulsen and B. Albinsson, *J. Am. Chem. Soc.*, 2022, **144**, 3706–3716.

56 C. Brand, W. L. Meerts and M. Schmitt, *J. Phys. Chem. A*, 2011, **115**, 9612–9619.

57 P. Kimbert and F. Plasser, *J. Chem. Theory Comput.*, 2023, **19**, 2340–2352.

58 Y. Murakami and K. Kamada, *Phys. Chem. Chem. Phys.*, 2021, **23**, 18268–18282.

59 Y. Zhou, F. N. Castellano, T. W. Schmidt and K. Hanson, *ACS Energy Lett.*, 2020, **5**, 2322–2326.

60 P. Baronas, J. Lekavičius, M. Majdecki, J. L. Elholm, K. Kazlauskas, P. Gaweł and K. Moth-Poulsen, *ACS Cent. Sci.*, 2025, **11**, 413–421.

61 E. Radiunas, L. Naimovičius, P. Baronas, A. Jozeliūnaitė, E. Orentas and K. Kazlauskas, *Adv. Opt. Mater.*, 2025, **13**, 2403032.

62 L. Naimovičius, S. K. Zhang and A. B. Pun, *J. Mater. Chem. C*, 2024, **12**, 18374–18380.

63 F. Edhborg, A. Olesund and B. Albinsson, *Photochem. Photobiol. Sci.*, 2022, **21**, 1143–1158.

64 A. J. Carrod, A. Cravcenco, C. Ye and K. Börjesson, *J. Mater. Chem. C*, 2022, **10**, 4923–4928.

65 Y. Sasaki, N. Yanai and N. Kimizuka, *Inorg. Chem.*, 2022, **61**, 5982–5990.

66 J.-H. Kim, C. E. Song, I.-N. Kang, W. S. Shind and D.-H. Hwang, *Chem. Commun.*, 2013, **49**, 3248–3250.

67 G. M. Sheldrick, *Acta Crystallogr., Sect. A: Found. Crystallogr.*, 2015, **71**, 3–8.

68 G. M. Sheldrick, *Acta Crystallogr., Sect. C: Struct. Chem.*, 2015, **71**, 3–8.

69 O. V. Dolomanov, L. J. Bourhis, R. J. Gildea, J. A. K. Howard and H. Puschmann, *J. Appl. Crystallogr.*, 2009, **42**, 339–341.

70 C. Adamo and V. Barone, *J. Chem. Phys.*, 1999, **110**, 6158–6170.



71 S. Grimme, J. Antony, S. Ehrlich and H. Krieg, *J. Chem. Phys.*, 2010, **132**, 154104.

72 E. R. Johnson and A. D. Becke, *J. Chem. Phys.*, 2005, **123**, 024101.

73 A. D. Becke and E. R. Johnson, *J. Chem. Phys.*, 2005, **123**, 154101.

74 R. Krishnan, J. S. Binkley, R. Seeger and J. A. Pople, *J. Chem. Phys.*, 1980, **72**, 650–654.

75 M. J. Frisch, G. W. Trucks, H. B. Schlegel, G. E. Scuseria, M. A. Robb, J. R. Cheeseman, G. Scalmani, V. Barone, G. A. Petersson, H. Nakatsuji, X. Li, M. Caricato, A. V. Marenich, J. Bloino, B. G. Janesko, R. Gomperts, B. Mennucci, H. P. Hratchian, J. V. Ortiz, A. F. Izmaylov, J. L. Sonnenberg, D. Williams-Young, F. Ding, F. Lipparini, F. Egidi, J. Goings, B. Peng, A. Petrone, T. Henderson, D. Ranasinghe, V. G. Zakrzewski, J. Gao, N. Rega, G. Zheng, W. Liang, M. Hada, M. Ehara, K. Toyota, R. Fukuda, J. Hasegawa, M. Ishida, T. Nakajima, Y. Honda, O. Kitao, H. Nakai, T. Vreven, K. Throssell, J. A. Montgomery Jr., J. E. Peralta, F. Ogliaro, M. J. Bearpark, J. J. Heyd, E. N. Brothers, K. N. Kudin, V. N. Staroverov, T. A. Keith, R. Kobayashi, J. Normand, K. Raghavachari, A. P. Rendell, J. C. Burant, S. S. Iyengar, J. Tomasi, M. Cossi, J. M. Millam, M. Klene, C. Adamo, R. Cammi, J. W. Ochterski, R. L. Martin, K. Morokuma, O. Farkas, J. B. Foresman and D. J. Fox, *Gaussian 16 Rev. C.01*, Wallingford, CT, 2016soft.

76 C. Lee, W. Yang and R. G. Parr, *Phys. Rev. B: Condens. Matter Mater. Phys.*, 1988, **37**, 785–789.

77 A. D. Becke, *J. Chem. Phys.*, 1993, **98**, 5648–5652.

78 M. R. Padhye, S. P. McGlynn and M. Kasha, *J. Chem. Phys.*, 1956, **24**, 588–594.

79 J. S. Brinen and J. G. Koren, *Chem. Phys. Lett.*, 1968, **2**, 671–672.

80 J. K. H. Pun, J. K. Gallaher, L. Frazer, S. K. K. Prasad, C. B. Dover, R. W. MacQueen and T. W. Schmidt, *J. Photonics Energy*, 2018, **8**, 1.

81 R. H. Clarke and R. M. Hochstrasser, *J. Mol. Spectrosc.*, 1969, **32**, 309–319.

82 E. M. Gholizadeh, S. K. K. Prasad, Z. L. Teh, T. Ishwara, S. Norman, A. J. Petty, J. H. Cole, S. Cheong, R. D. Tilley, J. E. Anthony, S. Huang and T. W. Schmidt, *Nat. Photonics*, 2020, **14**, 585–590.

83 T. N. Singh-Rachford and F. N. Castellano, *J. Phys. Chem. A*, 2008, **112**, 3550–3556.

84 J. C. De Mello, H. F. Wittmann and R. H. Friend, *Adv. Mater.*, 1997, 230–232.

